Ultra-portable field transfer radiometer for vicarious calibration of earth imaging sensors

Kurtis Thome[1], Brian Wenny[2], Nikolaus Anderson[3], Joel McCorkel[1], Jeffrey Czapla-Myers[3], and Stuart Biggar[3]

[1]*NASA Goddard Space Flight Center, Greenbelt, MD, USA,* [2]*Science Systems & Applications, Inc., Lanham, MD, USA,*
[3]*College of Optical Sciences, University of Arizona, Tucson, AZ, USA*
Corresponding e-mail address: kurtis.thome@nasa.gov

A small portable transfer radiometer has been developed as part of an effort to ensure the quality of upwelling radiance from test sites used for vicarious calibration in the solar reflective. The test sites are used to predict top-of-atmosphere reflectance relying on ground-based measurements of the atmosphere and surface. The portable transfer radiometer is designed for one-person operation for on-site field calibration of instrumentation used to determine ground-leaving radiance. The current work describes the detector- and source-based radiometric calibration of the transfer radiometer highlighting the expected accuracy and SI-traceability. The results indicate differences between the detector-based and source-based results greater than the combined uncertainties of the approaches. Results from recent field deployments of the transfer radiometer using a solar radiation based calibration agree with the source-based laboratory calibration within the combined uncertainties of the methods. The detector-based results show a significant difference to the solar-based calibration. The source-based calibration is used as the basis for a radiance-based calibration of the Landsat-8 Operational Land Imager that agrees with the OLI calibration to within the uncertainties of the methods.

1. INTRODUCTION

The starting point for accurate, on-orbit data from earth imagers is the significant effort made in the laboratory for pre-launch characterization and calibration. Such efforts are necessary to ensure the quality of the on-orbit data and to understand unexpected features to the data. On-orbit calibration approaches provide additional information to understand the imager's behavior. Radiometric calibration is a key element of the on-orbit assessment to determine any optical or other sensor degradation in going to orbit or while the sensor is on orbit. Vicarious calibration approaches have been shown to provide both relative [Heidinger et al., 2002; Ardanuy et al., 2006; Vermote and Saleous, 2006; Teillet et al., 2007; Wu et al., 2008; Goldberg et al., 2011; Doelling et al., 2013; Wu et al., 2013] and absolute radiometric calibration [Hovis et al., 1985; Slater et al., 1987; Abel et al., 1993; Bruegge et al., 2002; Guenther et al., 2002; Kneubuehler, 2003; Govaerts, 2004; Markham et al., 2004; Thome, 2004; Thome et al., 2003; Helder, 2008; Thome et al. 2008; Czapla-Myers et al., 2010]. In-situ based, vicarious approaches have played a role to provide absolute radiometric calibration since the late 1980s [Slater et al., 1987; Bruegge et al., 2002; Kneubuehler, 2003; Thome, 2004; Thome et al., 2003; Helder, 2008; Thome et al. 2008; Czapla-Myers et al., 2010]. The primary advantage to the in-situ approaches relative to the on-board calibrators and pseudo-invariant site relative calibrations is that they provide an absolute radiometric calibration with well-established error budgets and traceability to SI and national scales [Biggar et al., 1994; Thome et al., 2005].

Developing the error budgets and demonstrating SI-traceability for in-situ based vicarious results is a key element to allowing results from multiple groups and test sites to be combined to provide a more comprehensive understanding of the imager. Round-robin activities and joint field campaigns have provided a basis for developing and verifying the error budgets [Thome et al., 1998; Thome et al., 2008a; Thome and Fox, 2011]. A joint campaign to Tuz Golu, Turkey led to the recommendation that:

> *A standardised radiometer should be developed that can act as transfer standard to link test-sites traceability* [Thome and Fox, 2011].

The above recommendation led the Remote Sensing Group (RSG) of the College of Optical Sciences at the University of Arizona to undertake development of a small portable transfer radiometer to act as a travelling transfer standard for vicarious calibration, [Anderson et al., 2015]. The field transfer radiometer would also serve to evaluate the temporal stability of the RSG's automated radiometers that are part of their Radiometric Calibration Test Site (RadCaTS) at the Railroad Valley Playa, USA [Czapla-Myers et al., 2010; Czapla-

Myers et al., 2012]. The design characteristics for the field transfer radiometer emphasized the instrument's use as a travelling standard and evaluating health of on-site field radiometers leading to a highly-portable radiometer with a high level of radiometric stability.

The current work describes briefly the reflectance-based and RadCaTS approaches to vicarious calibration as background to understand the field transfer radiometer specifications and use of the radiometer. An overview of the design of the Calibration Test Site SI-Traceable Transfer Radiometer (CaTSSITTR) is presented followed by the approaches used to characterize it, including the source-based, absolute radiometric calibration. CaTSSITTR characterization included assessments of linearity, signal-to-noise ratio, spectral response, and spatial response and show that it outperforms design requirements.

The results of the detector-based relative and absolute spectral response results are presented in Section 5 followed by field-based results from the deployment of CaTSSITTR to demonstrate its use in the field. The detector-based and source-based radiometric calibrations differ by more than the combined uncertainties of the methods. A solar-radiation-based calibration of CaTSSITTR shows consistency with the source-based results indicating a possible issue with the detector-based results.

A vicarious calibration of the Landsat-8 Operational Land Imager (OLI) using CaTSSITTR data at Railroad Valley is presented in Section 7 showing the utility of CaTSSITTR's portability. The results of the OLI calibration based on the source-based calibration show agreement with historical results from Railroad Valley. Further data are needed to understand the lack of consistency between the source-based calibration approaches with the detector-based method.

2. IN-SITU BASED VICARIOUS CALIBRATION

The reflectance-based, vicarious calibration approach is the underlying motivation for the work presented here. The reflectance-based method relies on measurements of the surface leaving radiance to derive a reflectance of the test site at approximately the same time that a sensor images the region. These surface measurements are combined with atmospheric measurements in a radiative transfer code to predict a radiance for the appropriate geometry and the spectral bandpasses of the sensor of interest. The approach is one of three vicarious methods developed in the late-1980s by the RSG [Slater et al., 1987; Biggar et al., 1990b]. Current levels of absolute uncertainties are at the 3% level with precision at the 1-2% level [Czapla-Myers et al., 2015; Thome et al., 2013; Thome et al. 2015].

The measurements for the reflectance-based method are normally made with personnel at the site. The test site reflectance is obtained from upwelling radiance measurements made by transporting a spectroradiometer across the test site. The measured radiances are converted to bi-directional reflectance factor (BRF) by ratio to measurements of upwelling radiance from a reference panel for which the BRF has been determined in the laboratory. Measurements of the reference are made periodically to account for sun angle and atmospheric changes.

The illumination and measurements relate strictly to a hemispheric-conical situation as opposed to BRF. The test sites and diffuser references have been chosen such that the change in BRF over the field of view of the field radiometers is small relative to other uncertainties. The sites are also selected to have low atmospheric aerosol loading such that the skylight irradiance relative to the direct solar irradiance is small even at shorter wavelengths. Further, the global, downwelling irradiance data is collected at the same time as the surface reflectance collections to indicate whether significant changes in diffuse skylight illumination occurred during the measurement period. The relative stability of the skylight illumination and near-lambertian quality of both the diffuser reference and test surface means that the uncertainties from treating the problem as a bi-directional one are much smaller than other uncertainties.

The field reference is characterized in the laboratory with against a standard of reflectance. Originally, the standard was pressed polytetrafluoroethylene based on a prescribed approach defined by National Institute of Standards and Technology (NIST) [Biggar et al., 1988] and more recently using a standard plaque calibrated in reflectance by NIST. Both approaches provide the NIST-traceability that ensures consistency with laboratory-based radiometric calibrations.

Atmospheric characterization data are collected at the same time as the surface reflectance measurements. The characterization relies on solar extinction measurements from a ten-band solar radiometer [Ehsani et al, 1998]. The solar radiometer is relatively calibrated in a Langley method scheme that also provides spectral

atmospheric optical depths [Gellman, et al. 1991]. More recently, optical depth data from an AERONET sun photometer have been used [Holben, 1998]. The retrieved optical depth is used as part of an inversion scheme to determine ozone optical depth and an aerosol size distribution that allows predicted atmospheric optical factors at the same wavelengths as the surface BRF results [Biggar et al., 1990a; Thome et al., 1992].

The atmospheric and surface data are inputs to a radiative transfer code that computes hyperspectral, at-sensor radiances [Thome et al., 1996; Berk et al., 2014]. The predicted output from the radiative transfer code is compared to the output of the sensor under test to provide the sensor calibration.

The reflectance-based approach has proven to be highly successful for the radiometric calibration of multiple sensors with varying spatial and spectral resolutions. The difficulty with the reflectance-based method is that it is highly labor intensive, requires significant investments in time getting to and from test sites, and cloudy conditions for the specific overpass can negate all of the efforts in attempting the approach. Automating the measurements reduces the effort required to do the calibrations while increasing the number of calibration opportunities [Czapla-Myers et al., 2012].

Automated collection led to the implementation of RadCaTS at Railroad Valley Playa with the basic philosophy being similar to the reflectance-based approach [Czapla-Myers et al., 2010]. Rather than transport a portable field spectrometer, a set of multispectral, downward-viewing radiometers are deployed at four locations on the playa viewing at nadir [Anderson et al., 2013]. The measured upwelling surface radiance reported by the ground viewing radiometers (GVRs) is combined with a computed downwelling irradiance based on atmospheric measurements to determine the surface reflectance for each individual band and playa location. An average surface reflectance is computed for each spectral band and these are combined with historical ground-based hyperspectral reflectance retrievals to determine a RadCaTS hyperspectral reflectance. The atmospheric parameters required for the atmospheric characterization are derived from AERONET sun photometers that have been in place at Railroad Valley since the 1990s. The automated approach has been shown to provide results of similar quality and accuracy as the reflectance-based approach [Czapla-Myers, 2012].

3. FIELD TRANSFER RADIOMETER

The reflectance retrieval of RadCaTS is based on the absolute radiometric calibration of the GVRs. It is this calibration that illustrates the importance of SI-traceability and the need to understand the GVR calibration as a function of time as there is no onboard calibration for the GVRs. The reflectance-based method itself benefits from in-field evaluations of the field diffuser reference and the field spectrometers. The field transfer radiometer, CaTSSITTR, was developed to provide an SI-traceable standard to validate the quality of the radiometric measurements for the in-situ vicarious methods.

The design of CaTSSITTR has been described previously [Anderson et al., 2015]. The radiometer has a single-aperture with seven commercial, off-the-shelf interference filters in a filter-wheel to provide spectral selection. The only optical elements in the radiometer are two precision apertures to define its 10° field of view (FOV). The apertures are machined from stainless steel as is the detector baseplate to minimize thermal expansion effects. Stainless steel also has the advantage of minimizing corrosion effects from operating in a field environment. The detector package is based on a single, silicon-based detector that, along with the electronics, is thermally stabilized to 308 K.

One goal for the instrument's design was to allow a single person to operate the instrument in the field. The deployment of the radiometer and its entire power and data acquisition system was to require only a single trip from the vehicle to the test site. Efficient data collection was also a key design driver while maintaining a level of absolute accuracy similar to that obtained in the laboratory. The primary goal for CaTSSITTR was to provide an on-site calibration of the GVRs at Railroad Valley Playa as well as other radiometers and references at other in situ vicarious calibration sites. The performance requirements based on the intended uses of CaTSSITTR are shown in Table I as well as results of laboratory testing of the instrument (Thome et al., 2017). The signal-to-noise ratio (SNR) specification was for signal levels expected during typical summer conditions at Railroad Valley Playa (0.3 reflectance and 30-degree solar zenith).

Table I. CaTSSITTR design requirements and characterization results						
	SNR	Linearity error	Stray light	Repeatability	Dark current variation	Spectral out-of-band
Requirement	>1000	<0.25%	<1%	>98% (24 months)	<0.001 of signal	<0.5%
Measured	>6700	<0.22%	<0.4%	>99.5% (days)	<0.00017 of signal	<0.5%

The opto-mechanical design follows the basic approach of the GVRs [Anderson et al., 2013] while focusing on size and weight reductions. As mentioned, CaTSSITTR has a single entrance aperture and relies on an eight-position filter wheel for spectral selection. One position in the filter wheel is dedicated to a filter "blank" to provide dark measurements. The other seven positions of the filter wheel are filled with commercial, off-the-shelf interference filters with nominal center wavelengths of 400, 450, 500, 550, 650, 850, 1000 nm with nominal 10- to 20-nm bandwidths.

Upgrading the GVR electronics to mimic the signal-related electronics of the previously-developed laboratory transfer radiometers ensures that CaTSSITTR has the data quality needed to operate as a field transfer [Biggar, 1998; Spyak et al., 2000; Anderson et al., 2008]. The electronics are mounted with space-grade thermal epoxy to a heated copper block to provide a stable 308 K operating temperature for critical electronic components, as well as the radiometer's silicon-based detector. Battery operation of the system provides clean power and the batteries are a compromise between small size for portability and large enough to provide a reasonable amount of time for data collection. The data acquisition system relies on a high-resolution voltage data logger coupled wirelessly to handheld storage devices.

Figure 1 shows a backside view of the radiometer and an image of the instrument being used at Railroad Valley Playa, Nevada in October 2016 including the operator to provide scale. The radiometer view shows the entire system excluding the data logger that mounts to the two pins that can be seen to the upper left of the radiometer. The deployed radiometer shows the data logger as well as the front aperture tube that is not visible in the backside view.

4. BROADBAND, SOURCE-BASED RADIOMETRIC CALIBRATION

Calibration and characterization of CaTSSITTR took place in the RSG's radiometric calibration facility. The characterization and results are described in detail [Thome et al., 2017] and an overview is presented here to describe the results shown in Table I. The testing made use of the expertise developed by RSG as part of its gonioradiometric measurements of diffuser panels [Biggar et al., 1988] as well as that used to characterize the transfer radiometers used in calibration round robin activities [Johnson et al., 1998; Yoon et al., 1998; Early et al., 2000].

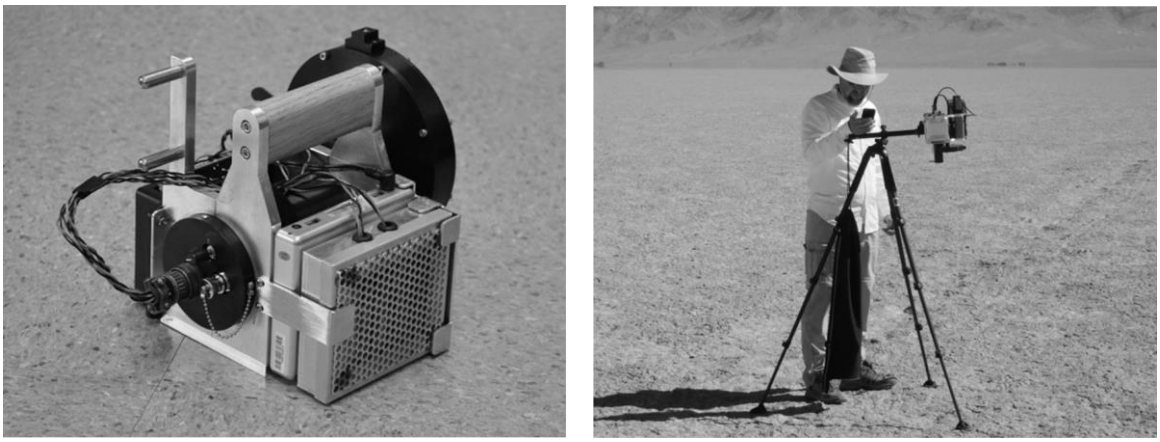

Figure 1. CaTSSITTR backside view and radiometer deployed at Railroad Valley Playa, Nevada

Linearity and SNR evaluation relied on a shutter-controlled spherical integrating source (SIS) that provides multiple source levels without significant changes in color temperature of the SIS output. Linearity for both radiometer gains as well as all spectral channels were evaluated from signal levels approximately three orders of magnitude lower to an order of magnitude larger than typical radiance values seen at vicarious calibration sites. CaTSSITTR met the required value shown in Table I for linearity by an order of magnitude except at the lowest radiance levels where the requirements were still met. SNRs determined for typical radiance levels for summer conditions at calibration sites far exceeded the requirements shown in Table I.

Repeatability of the radiometer was evaluated using the same SIS and consisted of repeated measurements on multiple occasions that included radiometer and source being disassembled, packed, and then set up. Measurements of the SIS output after multiple setup, measurement, and break down cycles show repeatability of 0.1% on the scale of hours and 0.5% over several days. Testing over longer time periods is still underway to demonstrate long-term repeatability and efforts are underway to understand whether it is the source, the source-sensor geometry, or CaTSSITTR behavior that is resulting in the 0.5% variation from day to day. The longer-term evaluations will give an indication as to whether the repeated use of the instrument in the field will require higher frequencies of laboratory calibrations and/or cleaning of the system.

The use of CaTSSITTR in the field will include views of smaller-sized reference samples than seen in the laboratory. The smaller samples will still subtend solid angles that are three times the designed FOV of CaTSSITTR, but it is important to ensure that sample measurements are not affected by out-of-field response. Ensuring a well-defined FOV is also necessary for evaluating field radiometers to understand the impacts of stray light response in those sensors. An out-of-field, stray light evaluation of CaTSSITTR based on a "lollipop" test demonstrated that the radiometer meets the required value of 0.01 for all spectral bands.

Dark current measurements recorded prior to, and after, each set of measurements show that dark current variation is well below the 0.001 requirement indicating the stability of the system's electronics. The advantage of a stable dark current is that it negates the need for repeated dark measurements and this allows for more efficient field collections. The collection efficiency, in turn, reduces uncertainties that can arise due to changes in atmospheric conditions or solar incidence angles with time.

Relative spectral response (RSR) of the radiometer was determined assuming that the spectral transmittance of the interference filters for each spectral band dominates the RSR. The transmittance of the filters was measured via a double monochromator system with both in-band sampling and an out-of-band sampling. The spectral out-of-band contribution was evaluated against lamp-based sources as well as the solar spectrum. All of the filters used in CaTSSITTR have noticeable out-of-band features, but none rise above the required value that indicates a significant out-of-band response for any of the spectral bands.

The last step in the laboratory characterization of CaTSSITTR was the absolute radiometric calibration using a NIST-calibrated irradiance lamp source and NIST-calibrated Spectralon® panel [Biggar 1998]. The absolute radiometric calibration was determined for each spectral band with absolute uncertainty < 2% (k=2) [Biggar 1998; Butler et al., 2003; Anderson et al., 2008; Thome et al., 2017].

5. NARROWBAND, DETECTOR-BASED RADIOMETRIC CALIBRATION

The portability of CaTSSITTR has allowed it to be characterized in the Goddard Laser for Absolute Measurement of Radiance (GLAMR) facilities at NASA's Goddard Space Flight Center. GLAMR is based on a detector-based approach to radiometric calibration [Angal et al., 2016]. GLAMR relies on a set of tunable lasers combined with detector-based traceability to determine the absolute radiance from a sphere source similar to the narrow-band, detector-based approach developed by NIST [Brown et al., 2004]. One advantage of GLAMR is that it can provide a full-field, near monochromatic source that allows determination of the absolute spectral response (ASR) with absolute uncertainties approaching 0.2% (k=2).

The SI-traceability of GLAMR is through the Primary Optical Watt Radiometer (POWR), a cryogenic electrical substitution radiometer that is the US standard for the electrical watt [Houston and Rice, 2006]. The traceability path follows that of NIST's Spectral Irradiance and Radiance Responsivity Calibrations using Uniform Sources (SIRCUS) [Brown et al., 2004]. The key to the traceability is a Gershun tube transfer radiometer that is calibrated using a tunable laser source that is characterized by POWR. The uncertainty of the radiometer calibration is 0.09% (k=3) [Brown et al., 2004]. GLAMR relies on a similar

set of transfer radiometers that are calibrated directly by NIST against POWR. The GLAMR transfer radiometers are used to monitor the output of the GLAMR tunable laser sources that have direct heritage to the SIRCUS system.

The GLAMR tunable laser sources can be coupled to a fiber optic that is further coupled to either a SIS to provide a radiance source or to a collimator to provide an irradiance source. The output of the source in either case is determined via the GLAMR transfer radiometers. The accuracy of such a radiance-based calibration has been demonstrated in NIST facilities to an expected accuracy of 0.2% for k=3 [Brown et al., 2004]. The radiance-based configuration is used for the calibration of CaTSSITTR.

A dual-monitoring approach is used for the calibration of CaTSSITTR in the GLAMR facility. The approach relies on a monitoring transfer radiometer that is mounted in the SIS. A second transfer radiometer is used to assess any systematic difference in the SIS output between the monitoring radiometer and the SIS exit-port view that CaTSSITTR uses during calibration. Evaluation of the GLAMR source temporal stability and the sphere uniformity indicates that this approach is suitable.

A window of opportunity to calibrate CaTSSITTR in the GLAMR facility occurred in February 2017 when the radiometer was at GSFC and an opening in the GLAMR schedule presented itself. Even so, the time-consuming nature of the measurements and other commitments for the laboratory allowed only the 850-nm spectral band to be characterized at the time of this publication. The 850-nm channel was selected because it allowed the GLAMR team to use the most efficient laser source in the system and that reduced the length of time needed for characterization. The wavelength range chosen also had the added benefit of maximizing the SNR for CaTSSITTR relative to other spectral bands and is less affected by out-of-band leaks when relying on tungsten-filament lamps for calibration. Finally, the part of the spectrum has been shown in past work to provide results that compare favorably to source-based methods (Johnson et al., 2003, Barnes et al., 2010).

The radiance from the SIS as determined by the GLAMR transfer radiometer for 199, near-monochromatic wavelengths between 800 and 900 nm is shown in Figure 2. Note that the units for Figure 2 are not spectral radiance. The laser-based illumination is relatively narrow in spectral width, but the data shown in Figure 2 are band-integrated values reported by the monitoring radiometer.

The dark-corrected output from CaTSSITR as a function of the wavelength of the GLAMR source is shown in Figure 3. The negative sign is simply a result of the polarity of the electronic system of CaTSSITTR. The spectral radiance and CaTSSITTR output are combined to determine the absolute spectral response (ASR) for each of the GLAMR spectral bands according to

$$ASR(\lambda_k) = \frac{S(\lambda_k)}{L(\lambda_k)} \tag{1}$$

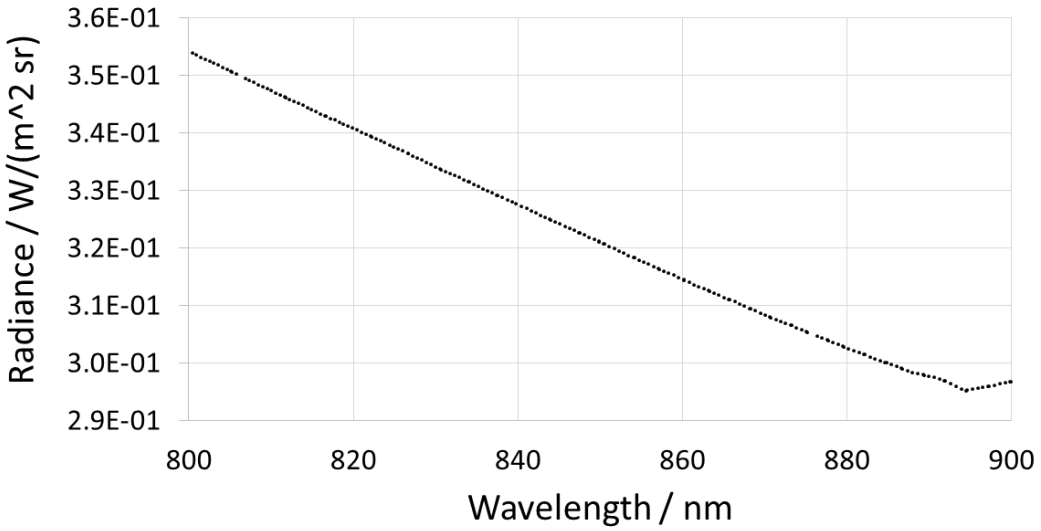

Figure 2. Radiance from GLAMR SIS reported by the monitoring transfer radiometer for the 199 wavelengths used for the CaTSSITTR calibration.

Where ASR(λ_k) is the absolute response at nominal GLAMR wavelength, λ_k, S is the dark-corrected output from CaTSITTR while viewing the GLAMR sphere source when tuned to wavelength λ_k, and L is the source radiance for that wavelength. The resulting ASR for CaTSSITTR is shown in Figure 4.

Of greater interest to the user is the gain of the CaTSSITTR spectral band for a broadband source that allows conversion of the CaTSSITTR output to a spectral radiance. The band-averaged, gain can be computed from the spectral ASR in similar fashion to Barnes et al. (2010) through a trapezoidal summation of the individual ASRs across the spectrum according to

$$g_i = \sum_{k=1}^{k_{max}} \frac{ASR_k + ASR_{k-1}}{2} [\lambda_k - \lambda_{k-1}] \quad (2)$$

where g_i is the gain of the i^{th} band of CaTSSITTR. Implementing (2) in this case assumes that the incident laser energy is narrow enough to be considered monochromatic and thus, ASR_k is a spectral ASR. Note that it is necessary to carry the wavelength difference for all terms because the tuning nature of the GLAMR source is such that it does not provide constant wavelength intervals.

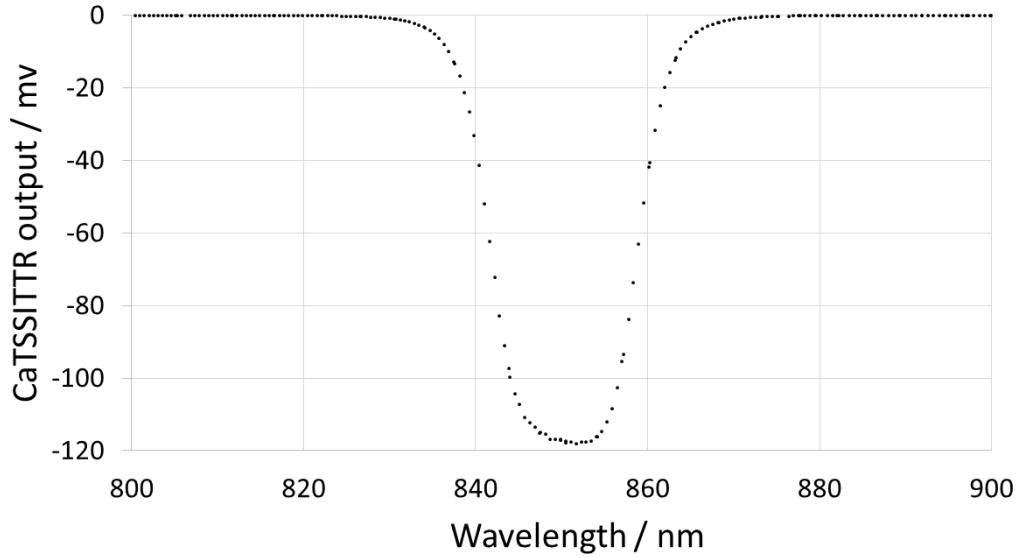

Figure 3. Output from CaTSSITTR while viewing the GLAMR SIS as it is tuned through 199 wavelengths between 800 and 900 nm

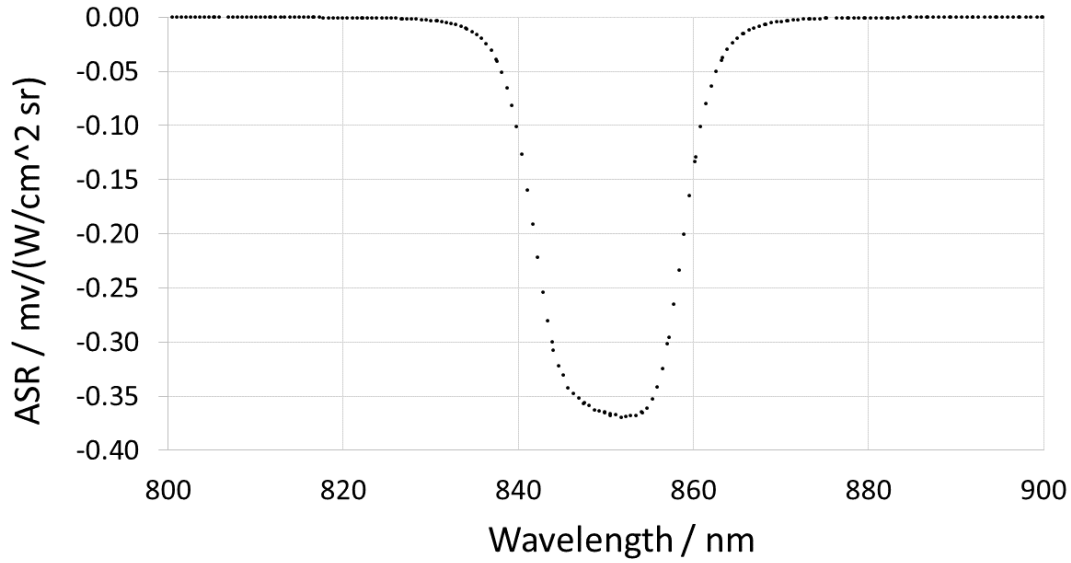

Figure 4. Retrieved CaTSSITTR ASR for each of the GLAMR source wavelengths

A bandwidth and band-averaged, center wavelength for the sensor helps to understand the spectral quality of the interference filters being used in CaTSSITTR. The band-averaged center wavelength, λ_c, for the radiometer is determined from [Barnes et al., 2010]

$$\lambda_c = \left[\sum_{k=1}^{k_{max}} \lambda_k ASR_k [\lambda_k - \lambda_{k-1}]\right] \Big/ \left[\sum_{k=1}^{k_{max}} ASR_k [\lambda_k - \lambda_{k-1}]\right] \quad (3)$$

Bandwidth is determined by normalizing to the ASR summation by the peak ASR [Barnes et al., 2010]

$$\Delta\lambda_i = \sum_{k=1}^{k_{max}} \frac{ASR_k}{ASR_{peak}} [\lambda_k - \lambda_{k-1}] \quad (4)$$

where ASR_{peak} is the maximum ASR (minimum in this case since the CaTSSITTR ASRs are negative) within the band of interest. The gain, center wavelength, and bandwidth for the CaTSSITTR band characterized with GLAMR are shown in Table II. The entries labeled "Incandescent source results" are the values obtained from the lamp-panel calibration and monochromator results described in the previous section that rely on incandescent lamps.

Table II. Absolute radiometric calibration and spectral results from detector- and source-based methods

	Gain $(W/m^2\ sr\ \mu m)/mV$	Center wavelength nm	Bandwidth nm
February 2017 GLAMR-based results	-148.2	850.7	18.3
September 2017 GLAMR-based results	-147.6	850.7	18.3
Incandescent source results	-139.7	850.5	18.5

The retrieved gains between the February 2017 GLAMR results and the incandescent source by 5.8% exceed the combined uncertainties of the two methods. Scheduling of the GLAMR system allowed a second collection of the 850-nm band and those results are shown as the September 2017 entry in the table. The gains retrieved for the two GLAMR runs agree to better than 0.4% and nearly identical values for bandwidth and center wavelength. It should be noted that the laser sources had been upgraded between the February and September collections but the same GLAMR transfer radiometers were used.

The large difference seen between the source and detector approaches is surprising given that past work has shown good agreement for this region of the spectrum (Johnson et al., 2003; Barnes et al., 2010). There is high confidence in the quality of the lamp-panel results as those have been shown to be in agreement with NIST through several round robin activities (Johnson et al., 1998, Yoon et al., 1998). A first check on the GLAMR data is to evaluate the retrieved relative spectral responses obtained from GLAMR and lamp-based data. The spectral results between the GLAMR and the monochromator systems are well within the uncertainties of the monochromator results giving a first indication that, from an integrated standpoint, the GLAMR data are of good quality.

An illustration of the spectral agreement between the monochromator and GLAMR data can be seen in Figure 5. Figure 5a shows the RSR over the full silicon-response range in logarithmic scale to show the out-of-band response. The GLAMR-based results are limited to the 800 to 900 nm spectral range due to time limitations of access to the GLAMR facility. The monochromator results span the full spectral range shown but are based on a component-level test of the CaTSSITTR interference filter only. The GLAMR results are at the instrument-level. Figures 5b and 5c show the in-band region of the measurements in log and linear scale. The agreement between the two measurement approaches indicate that GLAMR's detector monitors used to scale the sphere output are maintaining relative calibration over the time periods needed to perform an absolute calibration.

Details of the in-band results are shown in Figure 5d. The even sampling of the grating-based monochromator is apparent relative to the uneven sampling of GLAMR, as is the 1-nm interval of the

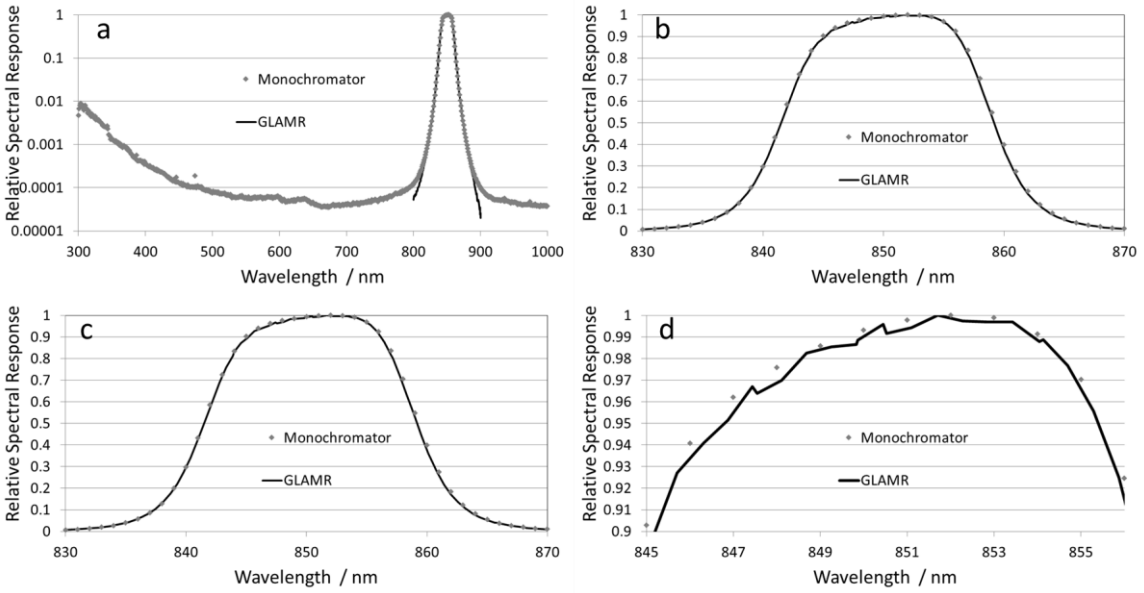

Figure 5. Comparison of the GLAMR and monochromator RSR results.

monochromator versus the approximately 0.5-nm interval for GLAMR. The uneven sampling is the result of GLAMR being limited to stable cavity modes and the automation of the tuning approach of the laser sources while optimizing the time to tune the laser. The monochromator data are smoother partially because of the broader bandwidth of the dual-grating monochromator source relative to the laser-based source of GLAMR. The laser-based nature of GLAMR can also induce interference effects and this has been postulated as an additional cause of the variability of the GLAMR-based RSRs.

What is clear in from Figure 5 is that the detector-based and source-based results are in excellent agreement in a relative sense. As further evaluation of the spectral data, the RSRs from both measurement approaches have been used to calculate a band-integrated lamp irradiance using the FEL spectral irradiance of the lamp source used in the lamp-panel calibration of Section 4. The band integrations agree to within 0.3% indicating that using the GLAMR RSR data would provide a lamp-panel calibration result that agrees with the monochromator results to within 0.3%.

The implication is that the cause of the nearly 6% difference between the detector-based and source-based gain results is not caused by differences in the spectral assessment of the CaTSSITTR response. A combination of the monochromator and GLAMR were used to determine whether the lack of full in-band and out-of-band GLAMR data could be the cause of the 6% difference. The monochromator-based out-of-band response was scaled using the maximum ASR from the GLAMR results to create a full spectrum ASR for CaTSSITTR. The retrieved gain in this case changed by only 0.4% from the in-band only case. The result is not a surprise since the spectral data shown in Figure 5a do not indicate a significant out-of-band leak.

The results shown in the remainder of the current work give reasonable confidence that CaTSSITTR is performing as expected when used with a broadband source and that there are no instrument-based features to cause the 6% effect. Studies are currently underway to evaluate the absolute knowledge of the radiance leaving the GLAMR SIS. The GLAMR team is evaluating possible interaction effects between the source and the radiometers under test. The absolute calibrations of the GLAMR transfer radiometers are being evaluated at NIST to determine whether there has been a shift in the radiometers scale. There is a concerted effort being made to include additional CaTSSITTR bands in the GLAMR laboratory, and comparison of CaTSSITTR to other radiometers.

6. FIELD DEPLOYMENT

The original intent of the field deployments was to evaluate the portability and stability of the CaTSSITTR. The initial CaTSSITTR deployment took place in October 2016, four months prior to the GLAMR calibrations. The data from this initial campaign not only demonstrated that CaTSSITTR meets its overall

design philosophy but has also been used to evaluate whether the instrument itself is the cause of the 6% discrepancy between the detector- and source-based results.

CaTSSITTR was deployed to the Railroad Valley test site in October 2016. A solar-radiation based calibration (SRBC) approach was used during the campaign to evaluate CaTSSITTR's laboratory radiometric calibrations and validate the radiometer's stability in going into the field. The SRBC is similar in philosophy to the lamp-panel method in that both rely on an irradiance source illuminating a diffuser reference that is viewed by the radiometer under study [Biggar et al., 1993]. The irradiance source for an SRBC is the sun and diffuser reference is essentially identical to that in the laboratory.

The SRBC method has been shown capable of providing high-accuracy radiance calibration for laboratory and field instruments [Anderson et al., 2007], as well as serving as a preflight calibration option for airborne and space borne imagers [Biggar et al., 1993; Barnes et al., 2000, Knight and Kvaran, 2014]. Past work has shown that SRBCs give radiometric calibrations that agree with laboratory calibrations to within the combined uncertainties of the two methods.

Figure 6 shows CaTSSITTR viewing a calibrated white reference at Railroad Valley Playa, Nevada. The sensor is viewing off-nadir by approximately five degrees to allow it to view at the same time as the GVR that is also shown. Typically, the SRBC approach has been used with a radiometer under test viewing the diffuser reference at a normal view. Past characterizations of the diffuser's BRDF indicate that the off-normal view has minimal impact on the overall SRBC accuracy.

One key difference between the lamp-panel method and SRBC is that there is the additional component of the skylight radiance in addition to the solar irradiance illumination. Figure 6 also shows the white reference being shaded from direct solar irradiance. Computing the difference between the CatSSITTR output when illuminated by the sun and skylight and that while shaded from the direct solar irradiance allows for removal of the diffuse sky irradiance leading to the predicted signal that CaTSSITTR would report if the diffuser were illuminated only by direct solar irradiance. Corrections for the small amount of forward scatter skylight that is also blocked along with the solar irradiance are small for the atmospheric conditions at Railroad Valley.

The other difference between the lamp-panel and SRBC is that transmittance along the lamp path is assumed to be unity while that along the solar path varies spectrally, temporally, and is significantly different from unity across the entire spectral range of CaTSSITTR. A correction for the effects of atmospheric scattering is developed from sun photometer measurements [Gellman et al. 1991]. Applying the transmittance correction in combination with an assumed solar spectral irradiance model allows the incident solar irradiance on the reflectance standard to be predicted.

Figure 6. CaTSSITTR and GVR viewing white reference as part of an SRBC collection at Railroad Valley Playa, Nevada. Right hand photo shows shading of the reference to provide measurement of diffuse skylight irradiance.

The BRF of the diffuser reference is determined in the laboratory relative to a NIST-calibrated standard of reflectance. The radiance onto CaTSSITTR is the product of the predicted solar irradiance and the panel BRF/π. The uncertainty of the radiance prediction has been shown to be <4.5% (k=2) with lower uncertainties at longer wavelengths [Thome et al., 2008b].

Three SRBC collections were made during the CaTSSITTR deployment to Railroad Valley Playa on October 5, 2016. The SRBCs took place as part of an intercomparison effort between CaTSSITTR and the RadCaTS GVRs and took place between 9:30 am and 2:00 pm local time. The three separate collections took place in three distinct locations meaning the diffuser reference was moved and leveled three times and CaTSSITTR was aligned to the panel three separate times.

Atmospheric transmittance was determined based on measurements from the on-site AERONET sun photometer. The aerosol optical depth, a measure of the column amount of aerosols, ranged from 0.035 to 0.037 at 500 nm for the three measurements. The values are typical of the low-aerosol conditions at Railroad Valley and are indicative of visibilities in excess of 100 km. Spectral dependence of the atmospheric transmittance follows a λ^{-4} for molecular scattering and is assumed to be $\lambda^{-\gamma}$ for aerosol scattering where γ is the Ångstrom turbidity coefficient. Values for γ ranged from 1.22 to 1.27, again typical values for the test site. The solar zenith angles were 45, 48, and 57 degrees for the three collections.

The solar zenith angle, atmospheric transmittance calculations were combined with the panel BRF and the solar model from Thuillier et al. [1998] to obtain predictions of the spectral radiance from the diffuser. The predicted spectral radiances were used to determine gain values for each CaTSSITTR spectral band as well as the average of all three cases. Figure 7 shows the gain for the three solar zenith angles relative to the average gain computed from all three SRBCs.

The agreement between the three solar-zenith cases is quite good with the standard deviation of the average < 1.0% for all bands as a result, in part, due to both the clear-sky and stable atmospheric conditions on the day of the measurements. No singular factor can be isolated as the cause of the small differences that are seen between the three results. One expected use of a high-quality field instrument such as CaTSSITTR is that its expected stability and radiometric quality should allow it to help pinpoint the causes of the differences seen in such data sets leading to improvements in the SRBC method.

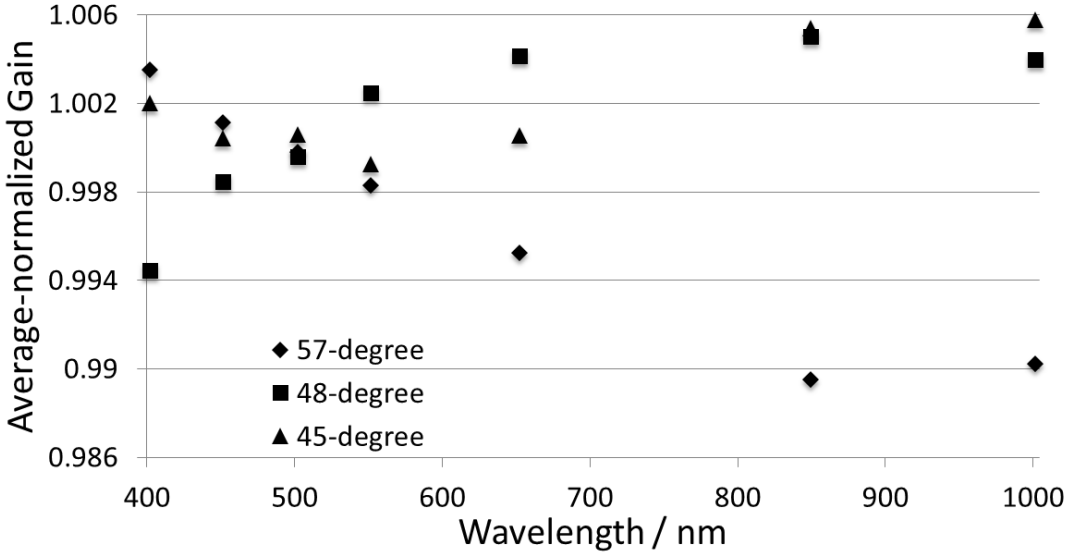

Figure 7. Normalized CaTSSITTR SRBC gains relative to average of three SRBC results.

Table III. CaTSSITTR gains by spectral band for three SRBCs, three source-based laboratory calibrations, and GLAMR detector-based calibration							
Wavelength / nm	CaTSSITTR gain (W/m^2 sr μm)/mV						
	SRBC 57°	SRBC 48°	SRBC 45°	FEL 330	FEL 560	SIS-based	GLAMR
400	-652.9	-647.0	-651.9	-658.0	-666.7	-672.3	
450	-312.1	-311.3	-311.9	-311.0	-315.3	-314.4	
500	-212.0	-212.0	-212.2	-211.3	-213.7	-213.9	
550	-198.1	-198.9	-198.3	-194.4	-196.4	-195.7	
650	-151.5	-152.9	-152.3	-149.0	-150.9	-149.6	
850	-141.0	-143.2	-143.2	-136.7	-139.7	-142.1	-148.2
1000	-115.2	-116.8	-117.0	-107.3	-110.4	-113.7	

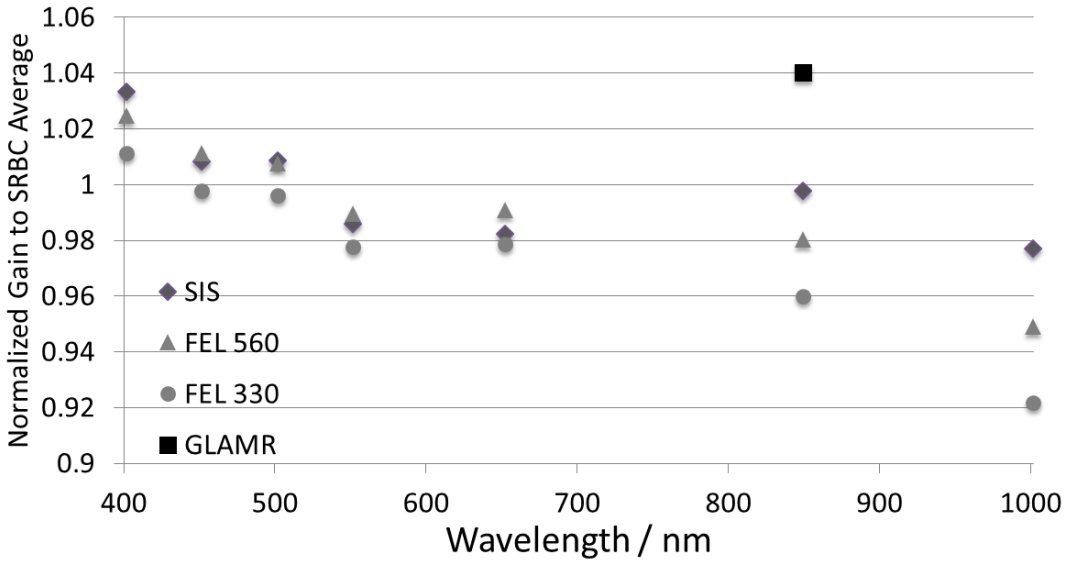

Figure 8. Results of three source-based absolute radiometric calibrations of CaTSSITTR and the GLAMR-based result at 850 nm relative to the average of the SRBC calibrations.

The SRBC results give confidence in using the average gain obtained from them as a reference for comparison of the results from the laboratory-based calibrations. Table III summarizes the retrieved gain from all of the SRBCs along with the CaTTSITTR gains from three source-based calibrations and the GLAMR-based result for the 850-nm spectral band. Figure 8 shows the laboratory-based gains relative to the average SRBC results.

The data labeled as FEL 330 and FEL 560 refer to two different FEL lamps obtained by RSG as primary standards of spectral irradiance from NIST. Both lamps were operated as part of lamp-panel calibrations of CaTSSITR to obtain the data in Table III and Figure 8. The SIS data points are based on the SIS used in the SNR and linearity characterization described in Section 4. The absolute spectral radiance from this SIS is based on a vendor-supplied absolute calibration. The vendor's calibration traces measurements of the SIS irradiance based on exit port size and distance to a laboratory spectroradiometer that transfers the spectral irradiance of a NIST standard FEL lamp.

The comparison results shown in Table II between GLAMR and the incandescent source are based on the FEL 560 results. FEL 560 is the newer of the two bulbs, though both are well within the 50-hour recommended operation limit for these standards. The FEL-based results agree with each other to within the combined absolute uncertainties of the FELs for wavelengths <800 nm. The larger differences at longer wavelengths are to be evaluated against a newer FEL standard once it is received by RSG. The lamp-panel FEL results agree with the SRBCs at all wavelengths to within combined uncertainties except for the FEL330 data point at 850 nm and both FELs at 1000 nm. The SIS results agree with the SRBC for all spectral bands while the GLAMR-based results disagree with the SRBCs at greater than the combined uncertainties.

The causes of the differences seen in Figure 8 are still under study, but indicate the utility of a system such as CaTSSITTR. The straightforward operation, compact design, ability to operate in the field, and radiometric properties of the radiometer make it an excellent tool to study the causes of differences seen in the comparisons presented here. One result that should be emphasized is that the lamp-panel calibration results for CaTSSITTR agree to well within the combined uncertainties to two independent calibration approaches. Admittedly, these two other approaches still ultimately trace back to incandescent standards from national laboratories, but it still points out that CaTSSITTR can be consistently calibrated with these multiple approaches.

7. RADIANCE-BASED SENSOR CALIBRATION

The deployment of CaTSSITTR to Railroad Valley Playa in October 2016 also offered the opportunity to collect data with CaTSSITTR for the radiance-based calibration of Landsat-8 Operational Land Imager. The radiance-based method is similar to the reflectance-based approach except that the measurements are not referred to a reflectance standard, but rather rely on the absolute radiometric calibration of the field sensor [Slater et al., 1987]. Past implementations used this approach with aircraft-mounted radiometers since there was no need for reference to the reflectance standard and it reduced uncertainties from the atmosphere [Biggar et al., 1994]. The approach offers another opportunity to evaluate the lamp-panel calibration against another radiometer that, in this case, is calibrated against a reflectance standard using a solar irradiance model similar to that used in Section 6.

The approach used here was to transport CaTSSITTR to 13 separate locations in a 500 m by 500 m area. Six points separated by approximately 100 m were located along a 500-m line oriented in an E-W direction. A similar sampling was performed along a second 500-m E-W path approximately 100 m to the north of the first line. The 13^{th} point was midway between the two lines at the western edge of the area. Data were collected for each spectral band and converted to spectral radiance using the FEL 560 lamp-panel calibration data.

The calibrated spectral radiance for each of the 13 locations is converted to spectral reflectance using atmospheric conditions obtained from the AERONET sun photometer located on the site. A single solar zenith angle was assumed to be representative of the entire 60 minutes of collection time as an initial approach to determine an at-sensor radiance. The MODTRAN radiative transfer code was run for the given solar zenith for a set of spectrally-flat surface reflectance values spanning the expected range of values for the Railroad Valley site. The outputs selected from MODTRAN were the top-of-the atmosphere and surface-leaving spectral radiances.

The surface-leaving spectral radiance is assumed to be linearly related to the surface reflectance, allowing a surface reflectance to be derived for each CaTSSITTR band and location through interpolation of the CaTSSITTR radiance to the surface-leaving radiances. The 13 surface reflectance values were averaged to give a reflectance valid for the 500 m by 500 m area. The resulting surface reflectance is shown in Figure 9 compared to the measured reflectance obtained by a field spectrometer operating in reflectance mode.

The multispectral surface reflectance values shown in Figure 9 were used as the basis for a hyperspectral reflectance interpolation covering 350 to 1000 nm at 1-nm intervals that relies on historical measurements of Railroad Valley reflectance using ground-based spectrometers. The interpolated, hyperspectral surface reflectance is used with an assumption of a linear relationship between the surface reflectance and top-of-atmosphere spectral radiance to compute a hyperspectral radiance at the OLI sensor based on the MODTRAN results for the Landast-8 overpass. The hyperspectral radiance is converted to spectral reflectance using the same solar irradiance model as the forward radiative transfer calculations.

The hyperspectral, top-of-atmosphere reflectance is band-averaged to the OLI bandpasses and compared to the OLI reflectance obtained from the imagery for that date and averaged over the 0.25 km^2 area. The results are presented in Figure 10. Also shown are the ratios of the predicted TOA reflectance from RadCaTS to OLI-based average values for 10 dates.

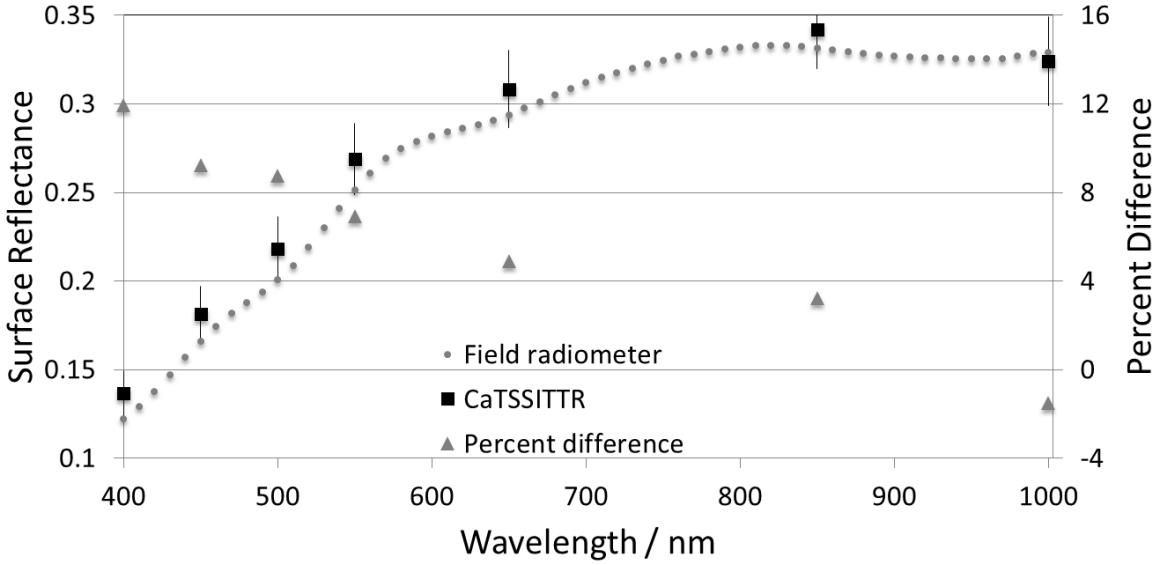

Figure 9. CaTSSITTR-derived surface reflectance for the 0.25 km^2 area of Railroad Valley Playa for the radiance-based calibration of Landsat-8 OLI. Also shown is the measured reflectance of the same area based on field spectrometer data collected in reflectance mode and the percent difference between spectrometer-based and CaTSSITTR-based results.

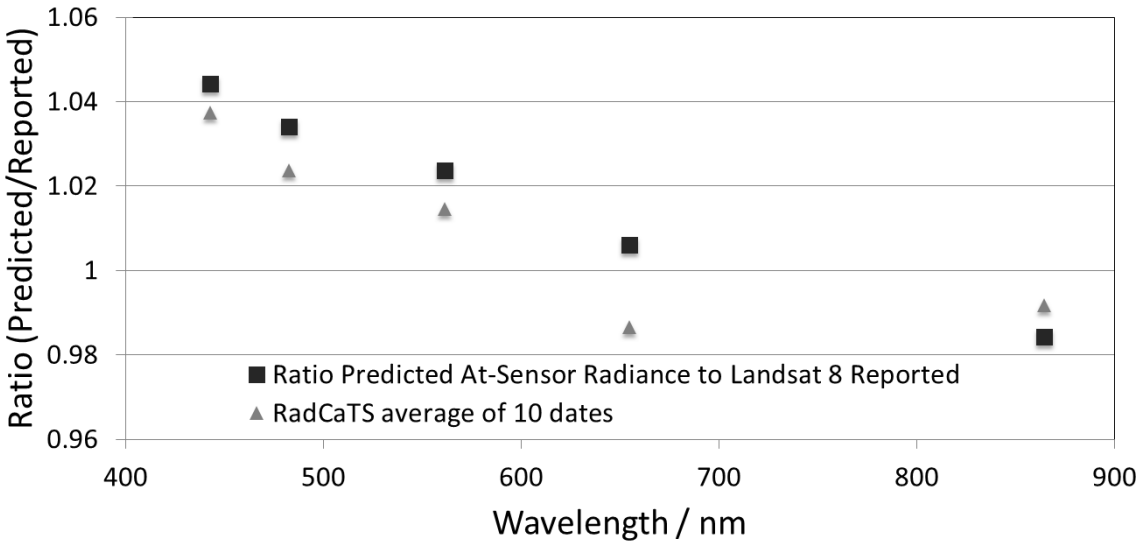

Figure 10. Ratio of predicted OLI radiance based on CaTSSITTR ground-based measurements to those reported for a 0.25 km^2 area of Railroad Valley Playa. Also shown are the average ratios based on 10 days of RadCaTS results from the 16 months prior to the CaTSSITTR-based values.

The immediate thing to note is that the remarkable agreement between the 10-day average from RadCaTS and the CaTSSITTR-based result. The agreement is to be expected since the RadCaTS GVRs and CaTSSITTR follow similar laboratory-calibration traceability, though the GVRs rely on a large-SIS that is calibrated to the lamp-panel calibrations based on a transfer spectroradiometer. The results indicate that the spatial sampling approach and the processing method developed for CaTSSITTR data are sufficient. It also indicates that the transfer radiometer has held its calibration in going from the laboratory to the field.

The radiance-based predictions from CaTSSITTR agree with the OLI-reported TOA reflectance to within the combined absolute uncertainties of the OLI calibration and the radiance-based method. The sloped shape to the ratios is currently under investigation, but the consistent shape between the OLI comparisons using both the GVRs and CaTSSITTR and the similar shape in the comparison with the SRBC results (Figure 8) point to a possible artifact in the lamp source calibration relative to other methods. Such an artifact could also

lead to the difference seen in the CaTSSITTR-based surface reflectance based on a radiance pathway relative to the field spectrometer results based on a reflectance pathway (Figure 9).

8. CONCLUSIONS

The characterization and calibration results for the field transfer radiometer presented here demonstrate the feasibility of developing stable, high-SNR, high-accuracy radiometers for use in characterizing field radiometers, field reference standards, and field sites being used in vicarious calibration. The laboratory results for CaTSSITTR show that it meets the requirements for linearity, out-of-band spectral response, stray-light rejection, SNR, dark current variability, and repeatability. Absolute radiometric calibration follows past approaches that are shown to have NIST-traceability to standards of spectral irradiance to better than 1.6% uncertainty (k=2).

The design of CaTSSITTR makes it highly suited for calibration using a range of methods including detector- and source-based methods. Limited availability of the GLAMR facility has allowed for only the 850-nm band of CaTSSITTR to be evaluated using detector-based approaches. The results from the GLAMR measurements of this band show excellent agreement in the relative spectral response between the GLAMR results and those from a lamp-based monochromator system. Unfortunately, the absolute radiometric calibration of CaTSSITTR disagrees by more than 5% between the GLAMR and lamp-panel approaches shown here. The lamp-panel results agree to well within the combined uncertainties of SRBC results as well as in comparison to OLI. Efforts are currently underway to understand the discrepancy between the lamp-panel results and those from GLAMR by calibrating additional channels and working with NIST to understand the absolute traceability of GLAMR.

The portability of CaTSSITTR was proven during an October 2016 field experiment to the RadCaTS site at Railroad Valley Playa, Nevada. SRBCs with CaTSSITTR show that the radiometer has maintained its absolute radiometric calibration into the field. The radiance-based calibration of Landsat-8 OLI using CaTSSITTR demonstrates the validity of the OLI radiometric calibration as well as the utility of field transfer radiometers to characterize field test sites and provide standards for vicarious calibration. Further use of systems like CaTSSITTR will both improve knowledge of the test sites as well as provide the accurate data needed to decouple atmospheric, surface, and processing uncertainties.

Additionally, the portability of CaTSSITTR will allow it to be transported to multiple locations increasing the number of traceable test sites for vicarious calibration, both those with automated instrumentation as well as those without. It is expected that CaTSSITTR, and other instruments like it that meet the Tuz Golu recommendation, will ensure that data from multiple sites will be harmonized to allow networking of the data from multiple test sites such as that planned by the Radiometric Calibration Network (RadCalNet) that is part of the Committee on Earth Observation Satellites' (CEOS) Working Group on Calibration and Validation (WGCV). Such efforts become more important as the numbers of on-orbit imaging sensors continues to increase and the users of these data expand their applications to include multiple sensors from multiple agencies and commercial providers. Networked test sites provide the capability to place these multiple sensors on a consistent scale while instruments such as CaTSSITTR will be used to do the same for the test sites.

9. REFERENCES

P. Abel, B. Guenther, R. N. Galimore, J. W. Cooper, "Calibration results for NOAA-11 AVHRR Channels 1 and 2 from Congruent Path Aircraft Observations," *Journal Atmos. and Oceanic Tech.*, **10**, 493-508, 1993.

N. Anderson, S. Biggar, K. J. Thome, and N. Leisso, "Solar radiation-based calibration of laboratory grade radiometers," *Proc. of SPIE 6677*, **66770X**, 2007.

N. Anderson, K. J. Thome, K. J., Biggar, S. and Czapla-Myers, J. S., "Design and validation of a transfer radiometer." *Proc. of SPIE 7081*, **708104**, 2008.

N. Anderson, J. Czapla-Myers, N. Leisso, S. Biggar, C. Burkhart, R. Kingston, and K. Thome, "Design and calibration of field deployable ground-viewing radiometers," *Appl. Opt.*, **52,** 231-240, 2013.

N. Anderson, K. Thome, J. Czapla-Myers, S. Biggar, "Design of an ultra-portable field transfer radiometer supporting automated vicarious calibration," *Proc. SPIE 9607*, **960709**, 2015.

A. Angal, J. McCorkel, and K. Thome, “Evaluation of GLAMR-based calibration for SI-traceable field reflectance retrievals,” *Proc. SPIE 9972*, **99721U**, 2016.

P. Ardanuy, B. Bergen, A. Huang, G. Kratz, J. Puschell, C. Schueler, and J. Walker. “Simultaneous overpass off nadir (SOON): A method for unified calibration/validation across IEOS and GEOSS system of systems,” *Proc. SPIE 6301*, **630101**, 2006.

R. A. Barnes, R. E. Eplee, Jr., S. F. Biggar, K. J. Thome, E. F. Zalewski, P. N. Slater, and A. W. Holmes, “SeaWiFS transfer-to-orbit experiment,” *Appl. Opt.*, **39,** 5620-5631, 2000.

R. A. Barnes, S. W. Brown, K. R. Lykke, B. Guenther, X. Xiong, J. J. Butler, "Comparison of two methodologies for calibrating satellite instruments in the visible and near infrared", *Proc. SPIE 7862*, **78620C**, 2010.

A. Berk, P. Conforti, R. Kennett, T. Perkins, F. Hawes, J. van den Bosch, "MODTRAN6: a major upgrade of the MODTRAN radiative transfer code", *Proc. SPIE 9088*, **90880H**, 2014.

S. F. Biggar, J. F. Labed J. F., Santer R. P., Slater P. N., Jackson R. D., and Moran, M. S., “Laboratory calibration of field reflectance panels,”*Proc. SPIE 924*, 232-240, 1988.

S. F. Biggar, D. I. Gellman, and P. N. Slater, “Improved evaluation of optical depth components from Langley plot data.” *Rem. Sens Env*, **32**, 91-101, 1990a.

S. F. Biggar, R. P. Santer, and P. N. Slater, “Irradiance-based calibration of imaging sensors,” *Proc. IGARSS*, 507-509, 1990b.

S. F. Biggar, P. N. Slater, K. J. Thome, A. W. Holmes, and R. A. Barnes, "Preflight solar-based calibration of SeaWiFS," *Proc. SPIE 1939*, 233-242, 1993.

S. F. Biggar, P. N. Slater, and D. I. Gellman, “Uncertainties in the in-flight calibration of sensors with reference to measured ground sites in the 0.4-1.1 μm range,” *Rem. Sens. Env,* **48**, 242-252, 1994.

S. Biggar, “Calibration of a visible and near-infrared portable transfer radiometer,” *Metrologia*, **35**, 701-706, 1998.

S. Brown, G. Eppeldauer, and K. Lykke, “Facility for spectral irradiance and radiance responsivity calibrations using uniform sources.” *Appl. Opt.*, **45**, 2006

C. J. Bruegge, N. L. Chrien, R. R. Ando, D. J. Diner, W. A. Abdou, M. C. Helmlinger, S. H. Pilorsz, K. J. Thome, “Early validation of the Multi-angle Imaging Spectroradiometer (MISR) radiometric scale,” *IEEE Trans. Geosci. Remote Sens.*, **40**, 1477-1492, 2002.

J. J. Butler, and R. A. Barnes, “The use of transfer radiometers in validating the visible to shortwave infrared calibrations of radiance sources used by instruments in NASA’s Earth Observing System,” *Metrologia*, **40**, 570-577, 2003.

J. S. Czapla-Myers, K. J. Thome, and N. P. Leisso, “Radiometric calibration of earth-observing sensors using an automated test site at Railroad Valley, Nevada,” *Can. J. Remote Sensing*, **36**, 474-487, 2010.

J. S. Czapla-Myers, N. P. Leisso, N. J. Anderson, and S. F. Biggar, “On-orbit radiometric calibration of Earth-observing sensors using the Radiometric Calibration Test Site (RadCaTS),” *Proc. SPIE 8390*, **83902B**, 2012.

J. Czapla-Myers, J. McCorkel, N. Anderson, K. J. Thome, S. Biggar, D. Helder, D. Aaron, L. Leigh, and N. Mishra. "The Ground-Based Absolute Radiometric Calibration of Landsat 8 OLI." *Remote Sens.*, **7,** 600-626, 2015.

D. R. Doelling, D. Morstad, B. R. Scarino, R. Bhatt, and A. Gopalan, “The characterization of deep convective clouds as an invariant calibration target and as a visible calibration technique,” *IEEE Trans. Geosci. Remote Sens.*, **51**, 1147–1159, 2013.

E. A. Early, P. Y. Barnes, B. C. Johnson, J. J. Butler, C. J. Bruegge, S. F. Biggar, P. R.Spyak, and M. M. Pavlov, “Bidirectional reflectance round-robin in support of the Earth Observing System program,” *J. Atmos. and Oceanic Tech.* **17**, 1077-1091, 2000.

A. R. Ehsani, J. A. Reagan, and W. H. Erxleben, “Design and performance analysis of an automated 10-channel solar radiometer instrument,”*Journal of Atmos. and Oceanic Tech.*, **15**, 697-707, 1998.

D. I. Gellman, S. F. Biggar, P. N. Slater, and C. J. Bruegge, “Calibrated intercepts for solar radiometers used in remote sensor calibration,” *Proc. SPIE 1493*, 175-180, 1991.

M. Goldberg, G. Ohring, J. Butler, C. Cao, R. Datla, D. Doelling, V. Gärtner, T. Hewison, B. Iacovazzi, D. Kim, T. Kurino, J. Lafeuille, P. Minnis, D. Renaut, J. Schmetz, D. Tobin, L. Wang, F. Weng, X. Wu, F. Yu, P. Zhang, and T. Zhu, “The Global Space-Based Inter-Calibration System (GSICS),” *Bull. Amer. Meterorol. Soc.*, **92**, 467–475, 2011.

Y. M. Govaerts, M. Clerici, and N. Clerbaux, “Operational calibration of the Meteosat radiometer VIS band,” *IEEE Trans. Geosci. Remote Sens.*, **42**, 1900-1914, 2004.

B. Guenther, X. Xiong, V. V. Salomonson, W. L. Barnes, J. Young, J., "On-orbit performance of the Earth Observing System Moderate Resolution Imaging Spectroradiometer; first year of data," *Rem. Sens. Env.*, **83**, 16-30, 2002.

A. K. Heidinger, C. Cao, and J. T. Sullivan, "Using Moderate Resolution Imaging Spectrometer (MODIS) to calibrate advance very high resolution radiometer reflectance channels," *Journal of Geophys. Res*, **107**, 4702-4704, 2002.

D. L. Helder, B. L. Markham, K. J. Thome, J. A. Barsi, G. Chander, R. Malla, "Updated radiometric calibration for the Landsat-5 Thematic Mapper reflective bands," *IEEE Trans. Geosci. Remote Sens.*, **46,** 3309-3325, 2008.

B. N. Holben, T. F. Eck, I. Slutsker, D. Tanre, J. P. Buis, A. Setzer, E. Vermote, J. A. Reagan, Y. Kaufman, T. Nakajima, F. Lavenu, I. Jankowiak, and A. Smirnov, "AERONET - A federated instrument network and data archive for aerosol characterization," *Rem. Sens. Env.*, **66**, 1-16, 1998.

J. M. Houston and J. P. Rice, NIST reference cryogenic radiometer designed for versatile performance, *Metrologia*, **43**, S31-S35, 2006.

W. A. Hovis, J. S. Knoll, and G. R. Smith, "Aircraft measurements for calibration of an orbiting spacecraft sensor," *Appl. Opt.*, **24**, 407-410, 1985.

B. C. Johnson, P. Y. Barnes, T. R. O'Brian, J. J. Butler, C. J. Bruegge, S. Biggar, P. R. Spyak, and M. M. Pavlov, "Initial results of the bidirectional reflectance characterization round-robin in support of EOS," *Metrologia*, **35**, 609-613, 1998.

B. C. Johnson, S. W. Brown, G. P. Eppeldauer, and K. R. Lykke, "System-level calibration of a transfer radiometer used to validate EOS radiance scales," *Int. J. Remote Sensing*, **24,** 339-356, 2003.

M. Kneubuehler, M. E. Schaepman, K. J. Thome, and D. R. Schlapfer, "MERIS/ENVISAT vicarious calibration over land," *Proc. SPIE 5234*, 614-623, 2003.

E. J. Knight and G. Kvaran, "Landsat-8 Operational Land Imager Design, Characterization, and Performance," *Remote Sens.*, **6**, 10286-10305, 2014.

B. L. Markham, K. J. Thome, J. A. Barsi, E. Kaita, D. L. Helder, J. L. Barker, and P. L. Scarmuzza, "Landsat-7 ETM+ on-orbit reflective band radiometric stability and absolute calibration," *IEEE Trans. Geosci. Remote Sens.*, **42**, 2810-2820, 2004.

P. R. Spyak, D. S. Smith, J. Thiry, and C. Burkhart, "Short-wave infrared transfer radiometer for the calibration of the Moderate-Resolution Imaging Spectrometer and the Advanced Spaceborne Thermal Emission and Reflection Radiometer," *Appl. Opt.*, **31**, 5694-5706, 2000.

P. M. Teillet, G. Fedosejevs, K. Thome, J. L. Barker, "Impacts of spectral band difference effects on radiometric cross-calibration between satellite sensors in the solar-reflective spectral domain," *Rem. Sens. Env.*, **110**, 393-409, 2007.

P. N. Slater., S. F. Biggar, R. G. Holm, R. D. Jackson, Y. Mao, M. S. Moran, J. M. Palmer, and B. Yuan, "Reflectance- and radiance-based methods for the in-flight absolute calibration of multispectral sensors," *Rem. Sens. Env*. **22,** 11-37, 1987.

K. Thome, B. Herman, J. Reagan, "Determination of precipitable water from solar transmission," *J. Appl. Met*., **31**,157-165, 1992

K. J. Thome, C. L. Gustafson-Bold, P. N. Slater, and W. H. Farrand, "In-flight radiometric calibration of HYDICE using a reflectance-based approach," *Proc. SPIE 2821*, 311-319, 1996.

K. J. Thome, S. Schiller, J. Conel, K. Arai, and S. Tsuchida, S., "Results of the 1996 Earth Observing System vicarious calibration campaign at Lunar Lake Playa, Nevada (USA)." *Metrologia*, **35**, 631-638, 1998.

K. J. Thome, S. F. Biggar, W. T. Wisniewski, "Cross-comparison of EO-1 sensors and other Earth Resources Sensors to Landsat-7 ETM+ Using Railroad Valley Playa*," IEEE Trans. Geosci. Remote Sens.*, **41**, 1180-1188, 2003.

K. J. Thome, "In-flight intersensor radiometric calibration using vicarious approaches," Post-Launch Calibration of Satellite Sensors, Edited by S. A. Morain and A. M. Budge, Balkema Publishers, Philadephia, 93-102, 2004.

K. J. Thome, C. Catrall, J. DAmico, and J. Geis. "Ground-reference calibration results for Landsat-7 ETM+." *Proc. of SPIE 5882*, **58820B**, 2005.

K. J. Thome, K. Arai, S. Tsuchida, and S. Biggar, "Vicarious calibration of ASTER via the reflectance-based approach." *IEEE Trans. Geosci. Remote Sens.*, **46**, 3285-3295, 2008a.

K. J. Thome, J. Czapla-Myers, M. Kuester, and N. Anderson, "Accuracy assessment for the radiometric calibration of imaging sensors using preflight techniques relying on the sun as a source." *Proc. SPIE 7081*, **708118**, 2008b.

K. J. Thome and N. Fox, "2010 CEOS field reflectance intercomparisons lessons learned," *Proc. IEEE IGARSS*, 3879-3883, 2011.

K. J. Thome, J. McCorkel, and J. Czapla-Myers. "In-Situ Transfer Standard and Coincident-View Intercomparisons for Sensor Cross-Calibration." *IEEE Trans. Geosci. Remote Sens.*, **51,** 1088-1097, 2013.

K. Thome, J. Czapla-Myers, B. Wenny, N. Anderson, "Calibration and use of an ultra-portable field transfer radiometer for automated vicarious calibration", *Proc. SPIE 10402*, **104020L**, 2017.

Thuillier, G., Herse, M., Simon, P. C., Labs, D., Mandel, H., Gillotay, G. and T. Foulols, "The visible solar spectral irradiance from 350 to 850 nm as measured by the SOLSPEC spectrometer during the ATLAS-1 mission," *Solar Physics* **177**, 41-61, 1998.

E. F. Vermote, and N. Z. Saleous, "Calibration of NOAA-16 AVHRR over a desert site using MODIS data," *Rem. Sens. Env.,* **105**, 214-220, 2006.

A. Wu, X. Xiong, and C. Cao, "Terra and Aqua MODIS inter-comparison of three reflective solar bands using AVHRR onboard the NOAA-KLM satellites," *Int'l. Journal of Rem. Sens*, **29**, 1997-2010, 2008.

A. Wu, X. Xiong, D. R. Doelling, D. Morstad, A. Angal, and R. Bhatt, "Characterization of Terra and Aqua MODIS VIS, NIR, and SWIR spectral bands' calibration stability," *IEEE Trans. Geosci. Remote Sens.*, **51**, 4330–4338, 2013.

H. W. Yoon, B. C. Johnson, D. Kelch, S. Biggar, and P. R. Spyak, "A 400 nm to 2500 nm absolute spectral radiance comparison using filter radiometers," *Metrologia*, **35**, 563-568, 1998.